

# Processing of Multiple-Receiver Spaceborne Arrays for Wide-Area SAR

Nathan A. Goodman, *Student Member, IEEE*, Sih Chung Lin, Devindran Rajakrishna, and James M. Stiles, *Senior Member, IEEE*

**Abstract**—The instantaneous area illuminated by a single-aperture synthetic aperture radar (SAR) is fundamentally limited by the minimum SAR antenna area constraint. This limitation is due to the fact that the number of illuminated resolution cells cannot exceed the number of collected data samples. However, if spatial sampling is added through the use of multiple-receiver arrays, then the maximum unambiguous illumination area is increased because multiple beams can be formed to reject range-Doppler ambiguities. Furthermore, the maximum unambiguous illumination area increases with the number of receivers in the array.

One spaceborne implementation of multiple-aperture SAR that has been proposed is a constellation of formation-flying satellites. In this implementation, several satellites fly in a cluster and work together as a single coherent system. There are many advantages to the constellation implementation including cost benefits, graceful performance degradation, and the possibility of performing in multiple modes. The disadvantage is that the spatial samples provided by such a constellation will be sparse and irregularly spaced; consequently, traditional matched filtering produces unsatisfactory results.

We investigate SAR performance and processing of sparse, multiple-aperture arrays. Three filters are evaluated: the matched filter, maximum-likelihood filter, and minimum mean-squared error filter. It is shown that the maximum-likelihood and minimum mean-squared error filters can provide quality SAR images when operating on data obtained from sparse satellite constellations. We also investigate the performance of the three filters versus system parameters such as SNR, the number of receivers in the constellation, and satellite positioning error.

**Index Terms**—Array signal processing, multidimensional signal processing, radar, radar signal processing, random arrays, spaceborne radar, synthetic aperture radar.

## I. INTRODUCTION

A COMMONLY known design requirement for synthetic aperture radar (SAR) systems is the minimum SAR antenna area constraint [1]–[7]. The requirement arises because the illumination area of the ground must be restricted so that the radar does not receive ambiguous returns in range or Doppler. In spotlight mode, therefore, there is a maximum area that can be illuminated during a dwell. In stripmap mode, the width of the

SAR swath is restricted. Since illumination area and aperture size are inversely related, the maximum allowable illumination area corresponds to a minimum aperture size requirement.

It is desirable to increase the single-pass spotlight area or swathwidth of an SAR system. Increasing illumination area is advantageous for applications that immediately require a wide-area SAR map since fewer passes are needed to generate the image. For dynamic remote sensing applications that require wide coverage and monitoring over time, such as soil moisture, ecological, or oceanographic applications, increasing illumination area decreases revisit time. For these applications, short revisit times are crucial to maintaining valid information.

There have been many proposed solutions for increasing illumination area; however, most of them do so at the cost of degraded azimuth resolution. ScanSAR has been a popular method [1], [6]–[11] that uses this technique. In ScanSAR, the synthetic aperture size is limited, thereby reducing azimuth resolution but also allowing time for the beam to be scanned in elevation for multiple range swaths. One technique [5] changes the elevation dimension of the antenna in order to optimize the illumination area for different grazing angles, but the fundamental area limitation is still present. Another proposed method [12] uses multiple along-track beam positions and a larger along-track aperture. The method provides better SNR but does not improve revisit time for large areas. Several papers in the literature divide illumination time of a single receiver into smaller segments called subapertures, but this is done to null large side-lobe targets, improve processing efficiency, or reduce speckle [7], [10], [13]–[17]. Multiple looks from different off-nadir angles have also been proposed to improve range resolution [18]. Lastly, constellations of independent SAR satellites have been proposed [19] for reducing revisit time. This last approach reduces revisit time by optimizing the orbits of several independent SAR sensors, but the single-pass or instantaneous illumination area of each sensor is still limited.

In order to improve illumination coverage while maintaining azimuth resolution, multiple coherent receive apertures can be used [3], [11], [20], [21]. The illumination area is determined by the size of the individual apertures, and range-Doppler ambiguities that become illuminated are resolved through angle information provided to the system. The sum of the aperture areas must still satisfy the minimum area constraint; however, illumination area can be improved over the single-receiver case by a factor equal to the number of receivers.

Another reason for using multiple receive apertures is to mitigate the cost, fabrication, and deployment issues associated with placing a large spaceborne aperture into orbit [2], [22], [23].

Manuscript received November 9, 2001; revised December 4, 2001. This work was supported in part by the Air Force Office of Scientific Research under Contract F49620-99-1-0172.

N. A. Goodman, S. C. Lin, and J. M. Stiles are with the Radar Systems and Remote Sensing Laboratory, The University of Kansas, Lawrence, KS 66045 USA (e-mail: ngoodman@rsl.ku.edu).

D. Rajakrishna was with the Radar Systems and Remote Sensing Laboratory, The University of Kansas, Lawrence, KS 66045 USA. He is now with Tellabs, Inc., Lisle, IL 60532 USA.

Publisher Item Identifier S 0196-2892(02)04594-1.

When multiple receivers are employed, each receive aperture can be carried on a small separate satellite called a microsat. The reduced cost and deployment difficulties associated with these small satellites may make a constellation of formation-flying microsats more cost-effective than an equivalent large satellite [9], [22], [23]. Furthermore, the likelihood of system failure is reduced since failure will occur only to individual microsats, instead of a satellite carrying an entire system. If enough microsats fail such that performance is degraded below an acceptable level, replacement microsats can be *piggybacked* on other missions when room is available, thereby avoiding the cost of dedicated missions.

The microsat constellation concept also provides flexibility for performing in multiple modes and for multiple applications. The multi-angle SAR data could be used for a variety of applications including parameter estimation and jam-resistant communications [22]. Interferometric applications, such as terrain elevation mapping, would benefit from the constellation concept, and the effective size of a constellation would prove advantageous for space-based moving target indication.

Signal processing issues concerning the microsat concept stem from the fact that the satellites must be significantly spaced because the laws governing spaceborne formation flying only allow specific orbits. The array will have a wide spatial extent and will be sparsely sampled. It will be shown that, because of the sparse spatial sampling of the array, advanced algorithms must be used to process the spatial data.

The succeeding sections of this paper contain the mathematics needed for developing the processing algorithms and present simulations that demonstrate the performance benefits of multiple receive apertures. Other results demonstrate effective processing of sparsely populated spaceborne arrays. In Section II, we present a signal-space representation of the radar system that will be used to derive and graphically demonstrate the proposed algorithms. Section III provides results from single-aperture SAR and specifically demonstrates the need for multiple receive apertures. Section IV presents results for multiple receive apertures in a close, regularly spaced array, and multiple receive apertures in a sparsely populated array. Performance of different algorithms versus several system parameters is presented in Section V. Conclusions are provided in Section VI.

## II. SIGNAL-SPACE REPRESENTATION

The signal-space representation presented here encourages implementation of estimation algorithms through well-established linear algebra techniques and facilitates interpretation of the SAR filters that are used. The complex signal that a radar constellation measures,  $r(\mathbf{x}_r, t)$ , can be written as

$$r(\mathbf{x}_r, t) = \int_A \gamma_0(\mathbf{x}) \int_T h(\mathbf{x}_r, \mathbf{x}, t, t') s(t') dt' dA + n(\mathbf{x}_r, t) \quad (1)$$

where  $\mathbf{x}_r$  is the position vector to the receiver,  $\mathbf{x}$  is the position vector to a point on the ground,  $\gamma_0(\mathbf{x})$  is the complex reflectance per unit area at  $\mathbf{x}$ ,  $h(\mathbf{x}_r, \mathbf{x}, t, t')$  is a time-variant function describing the radar physics such as propagation and antenna gain,  $s(t')$  is the complex representation of the transmitted signal,  $T$

is the time over which the transmitted signal exists,  $A$  is the radar's illumination area, and  $n(\mathbf{x}_r, t)$  is complex noise. The integration in time is performed over the length of the transmit signal and is represented by  $\rho(\mathbf{x}_r, \mathbf{x}, t)$  to get

$$r(\mathbf{x}_r, t) = \int_A \gamma_0(\mathbf{x}) \rho(\mathbf{x}_r, \mathbf{x}, t) dA + n(\mathbf{x}_r, t). \quad (2)$$

Therefore, the response from a differential area on the ground, which depends on its position as well as the transmit signal, is characterized by  $\rho(\mathbf{x}_r, \mathbf{x}, t)$  to within a multiplicative constant. If the integration in (2) is approximated by a summation, the received signal becomes

$$r(\mathbf{x}_r, t) = \sum_i \gamma_0(\mathbf{x}_i) \rho(\mathbf{x}_r, \mathbf{x}_i, t) \Delta A + n(\mathbf{x}_r, t) \quad (3)$$

where the index  $i$  includes all discrete areas  $\Delta A$  that are illuminated and  $\mathbf{x}_i$  is the position vector to the center of the  $i$ th discrete area. If the signal is sampled in space according to the constellation and in time according to the signal's bandwidth, the  $m$ th sample at the  $n$ th receiver becomes

$$r(\mathbf{x}_r^n, t_m) = \sum_i \gamma_0(\mathbf{x}_i) \rho(\mathbf{x}_r^n, \mathbf{x}_i, t_m) \Delta A + n(\mathbf{x}_r^n, t_m). \quad (4)$$

Finally, the entire set of measurements can be represented using matrix-vector notation

$$\mathbf{r} = \mathbf{P}\boldsymbol{\gamma} + \mathbf{n} \quad (5)$$

where

$$\left. \begin{aligned} \mathbf{r} &= [r(\mathbf{x}_r^1, t_1) \quad r(\mathbf{x}_r^1, t_2) \quad \cdots \quad r(\mathbf{x}_r^N, t_{BT})]^\dagger \\ \mathbf{P} &= [\boldsymbol{\rho}_1 \quad \boldsymbol{\rho}_2 \quad \cdots \quad \boldsymbol{\rho}_M] \\ \boldsymbol{\gamma} &= [\gamma_1 \quad \gamma_2 \quad \cdots \quad \gamma_M]^\dagger \\ \mathbf{n} &= [n(\mathbf{x}_r^1, t_1) \quad n(\mathbf{x}_r^1, t_2) \quad \cdots \quad n(\mathbf{x}_r^N, t_{BT})]^\dagger \\ \boldsymbol{\rho}_i &= \\ &= [\rho(\mathbf{x}_r^1, \mathbf{x}_i, t_1) \quad \rho(\mathbf{x}_r^1, \mathbf{x}_i, t_2) \quad \cdots \quad \rho(\mathbf{x}_r^N, \mathbf{x}_i, t_{BT})]^\dagger \\ \gamma_i &= \gamma_0(\mathbf{x}_i) \end{aligned} \right\} \quad (6)$$

and  $(\cdot)^\dagger$  is the matrix or vector transpose. Also,  $BT$  is the received time-bandwidth product of a single receiver,  $N$  is the number of receivers in the constellation, and  $M$  is the number of resolution cells of size  $\Delta A$ . If the number of resolution cells  $M$  exceeds the number of measurements,  $NBT$ , then any solution to the complex RCS vector  $\boldsymbol{\gamma}$  will contain ambiguity.

Since the measurements contain noise, the SAR problem is one of estimating the values in the RCS vector  $\boldsymbol{\gamma}$ . As seen in (5), the radar process is approximated as linear; therefore, we seek an estimator that can be applied as a linear process. A weight vector, or filter, will be found for each resolution cell. When we take the inner product of the received measurements with each of the weight vectors, the estimated RCS vector  $\hat{\boldsymbol{\gamma}}$  is

$$\hat{\boldsymbol{\gamma}} = \mathbf{W}\mathbf{r} \quad (7)$$

where

$$\hat{\boldsymbol{\gamma}} = [\hat{\gamma}_1 \quad \hat{\gamma}_2 \quad \cdots \quad \hat{\gamma}_M]^\dagger \quad (8)$$

$$\mathbf{W} = [\mathbf{w}_1 \quad \mathbf{w}_2 \quad \cdots \quad \mathbf{w}_M]^\text{H} \quad (9)$$

$\mathbf{w}_i$  is the weight vector for the  $i$ th target, and  $(\cdot)^H$  denotes the conjugate-transpose operation. It is also important to note that this is the type of processing traditionally done in SAR, where  $\mathbf{w}_i$  is typically matched to measurements received from the  $i$ th resolution cell. Although some algorithms require more computation for finding each  $\mathbf{w}_i$ , the total size of  $\mathbf{W}$  remains constant; consequently, the data-dependent process of calculating inner products is equivalent for all linear estimators.

### III. SINGLE-APERTURE SAR

Ambiguities occur when the number of illuminated resolution cells exceeds the number of independent measurements collected. In spotlight mode, SAR focuses on a particular area for some time,  $T$ . During that time, independent complex samples can be collected at a maximum rate determined by the signal bandwidth  $B$ . Therefore, the maximum number of independent, complex samples that can be collected is equal to  $BT$ , also known as the time–bandwidth product. The problem is that bandwidth and observation time are fixed by the resolution requirements of the system. The range resolution requirement determines bandwidth, and the azimuth resolution requirement determines observation time. Since it is only possible to image unambiguously as many targets as there are independent samples, and since the number of independent samples is related through bandwidth and time to particular range and azimuth resolutions, the maximum imaging area is fixed. A simple example for a sidelooking, spotlight SAR is presented in the following. Suppose the resolution requirements imposed on the radar are  $\Delta x$  and  $\Delta R$  in azimuth and range, respectively. Range resolution is given by

$$\Delta R = \frac{c}{2B} \quad (10)$$

where  $c$  is the speed of light. For a  $90^\circ$  sidelooking geometry where the azimuth extent is small compared to the range, the azimuth resolution can be approximated as

$$\Delta x \approx \frac{\lambda_0 R_0}{2v} \frac{1}{T} \quad (11)$$

where  $\lambda_0$  is the wavelength at the center operating frequency,  $R_0$  is the average target range, and  $v$  is the along-track velocity of the radar platform. The area per pixel is then the product of the azimuth and range resolutions

$$\Delta x \Delta R = \frac{c \lambda_0 R_0}{4v} \frac{1}{BT}. \quad (12)$$

The maximum area is the time–bandwidth product multiplied by the area per pixel

$$A_{\max} = BT \Delta x \Delta R = \frac{c \lambda_0 R_0}{4v}. \quad (13)$$

As can be seen from the right side of (13), the maximum area that can be imaged is determined by range, wavelength, and platform velocity.

One solution appears to be increasing the time–bandwidth product. However, (10) and (11) clearly show that the resolution dimensions are inversely proportional to bandwidth and

time. For example, it is possible to get four times as many independent samples by increasing bandwidth and time each by a factor of two, but the resolution pixels would be half the original size on each side. This would result in four times as many samples, but the area of each pixel would be four times smaller, and the total area would remain the same. Radar designers sometimes stagger the transmit pulse repetition frequency (PRF) or apply other signal coding in order to modify the ambiguity function. However, the total energy in the ambiguity function must remain constant [24]. Therefore, these methods can rearrange ambiguity, but cannot make it disappear. It is impossible to get around the fact that more resolution cells are being illuminated than there are measurements available to distinguish them.

Fig. 1(a) shows the original SAR image used as the input to the simulations in this paper. Areas of zero scattering are indicated by black while areas of high scattering are indicated by white. If pixel values calculated through SAR processing are at or above the maximum scattering level in the input image, then they appear white in the processed image. Therefore, when scattering estimates become very large due to high input noise power, the visual representation of the output image becomes saturated with white. All ambiguity functions and array patterns, however, are represented as black on white in order to improve reproduction quality.

When a single aperture meets the minimum antenna area constraint, the number of illuminated resolution cells, or pixels, does not exceed the time–bandwidth product of the system, and the result is as shown in Fig. 1(b). However, if a larger area SAR map is desired, and the illumination area is increased for this reason, the result is as seen in Fig. 1(c). Another way of demonstrating why the poor result of Fig. 1(c) occurs is to determine the amount of correlation between all combinations of pixels. This is determined with the conjugate transpose of  $\mathbf{P}$  by

$$\mathbf{K} = |\mathbf{P}^H \mathbf{P}|. \quad (14)$$

The values on the diagonal of  $\mathbf{K}$  are the correlations of each target with itself; therefore, their values are the squared magnitude of the normalized measurement vectors. Off-diagonal elements,  $\mathbf{K}(i, j)$ , represent the amount of correlation, or ambiguity, between targets  $i$  and  $j$ . For example, the values in row one show how target one correlates with all other targets. The correlation matrix for a case where the number of illuminated targets exceeds the time–bandwidth product is shown in Fig. 1(d). It is seen in Fig. 1(d) that there are very dark off-diagonal elements; consequently, it is inferred that there is a large amount of correlation between some targets.

### IV. MULTIPLE-APERTURE SAR

A necessary requirement for increasing SAR map area is to increase the number of independent samples, or amount of information, that is collected without modifying resolution cell size in the process. It was shown that this is not possible by increasing bandwidth or illumination time. However, the amount of information collected can also be increased by adding information in the spatial domain. By adding more antenna apertures to the SAR system, each with its own receiver, angle-of-arrival

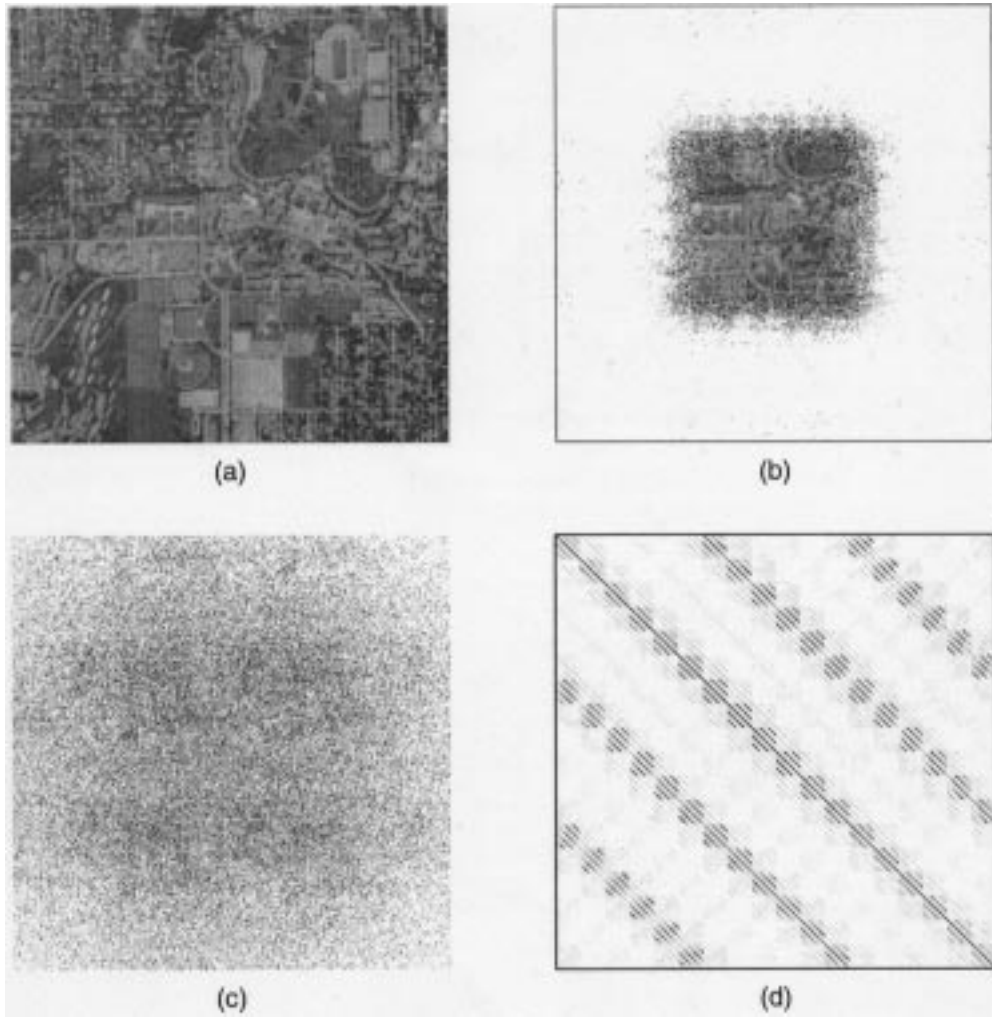


Fig. 1. Simulation results for a single-receiver SAR. (a) The original image is reconstructed from a system that (b) limits illumination by meeting the minimum antenna area constraint and one that (c) does not satisfy the minimum antenna area constraint. (d) The target correlation matrix for the case in (c) is shown.

information can be collected. If  $N$  is the total number of receive apertures, then the number of independent samples available to the system is now  $NBT$ . The maximum area is again the product of the number of independent samples and the area per pixel

$$A_{\max} = NBT\Delta x\Delta R = N\frac{c\lambda_0 R_0}{4v} \quad (15)$$

which is  $N$  times larger than was possible with a single receiver. Furthermore, it is noted that the angle-of-arrival information is unique from the time and frequency information, making it possible to discriminate between range-Doppler ambiguities. In other words, targets that are ambiguous in time and frequency (range-Doppler) will have different angles of arrival and can be distinguished.

Fig. 2 demonstrates how multiple receive apertures can resolve range-Doppler ambiguity. In this simulation, a single aperture that satisfied the minimum area constraint was divided into nine smaller apertures of equal size, each with a coherent receiver. In Fig. 2(a), the range-Doppler ambiguity function for a target is shown. From this figure it is apparent that for any target there are eight other targets that are ambiguous in the time and frequency domains. Fig. 2(b), however, shows the array

pattern when the array is focused on the center target. This is the spatial-domain ambiguity function for the center target. The eight targets that are ambiguous with the center target are located in the nulls of the array pattern. The total ambiguity function for the center target is, approximately, the product of the range-Doppler and spatial ambiguity functions. This product is shown in Fig. 2(c), which shows that the total ambiguity function approaches the ideal *thumbtack* shape. Energy from ambiguous targets has been eliminated rather than rearranged because of the addition of spatial information. Likewise, the correlation matrix for this scenario shown in Fig. 2(d) exhibits no significant off-diagonal elements, indicating that no ambiguities are present. The result for this method of processing applied to every target is shown in Fig. 3.

Figs. 2 and 3 demonstrate the effectiveness of multiple receive apertures. The question now becomes what is the best method of processing the newly added angle-of-arrival information for a given array formation.

#### A. Correlation Filter

Fig. 3 was generated using matched-filter, or correlation-filter, processing with nine receivers in a  $3 \times 3$  regular

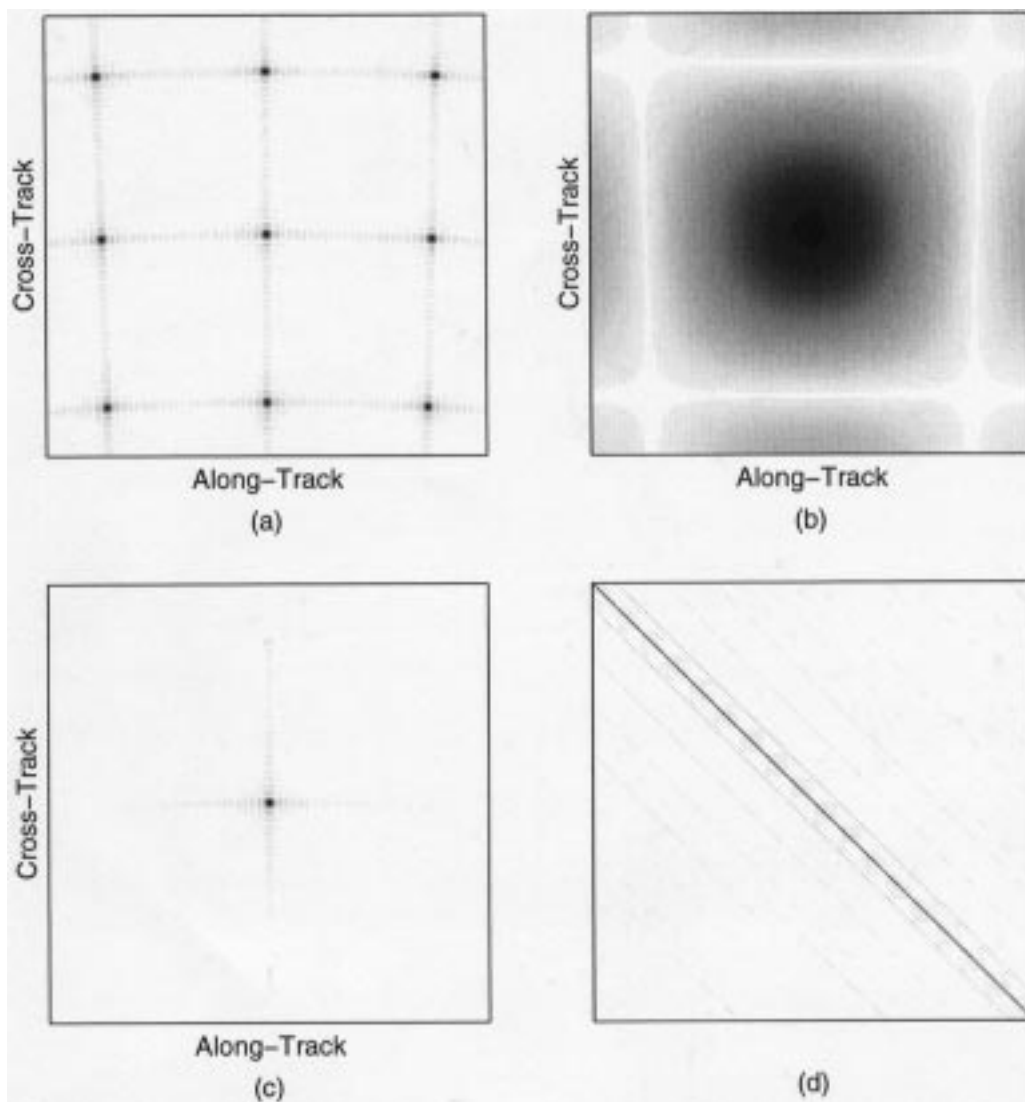


Fig. 2. Ambiguities in the (a) range-Doppler map fall on nulls in the (b) receive array pattern to approximately form the (c) total ambiguity function. (d) The target correlation matrix has no significant off-diagonal elements, demonstrating reduced ambiguity.



Fig. 3. SAR results using matched filter processing for a three-by-three closely spaced receiver array.

The vector representation of the correlation filter for the

$i$ th resolution cell is the weighted conjugate transpose of its measurement vector

$$\mathbf{w}_i^{\text{corr}} = \frac{\boldsymbol{\rho}_i}{|\boldsymbol{\rho}_i|^2} \tag{16}$$

where the superscript, corr, denotes that the filter is a correlation filter. If the matched filters for all resolution cells are placed into the columns of a matrix, the matched-filter estimator,  $\mathbf{W}_{\text{corr}}$ , is given by

$$\mathbf{W}_{\text{corr}} = \mathbf{D}^{-1} \mathbf{P}^H \tag{17}$$

where  $\mathbf{P}$  is described in (6), and  $\mathbf{D}$  is a diagonal matrix defined as

$$\mathbf{D} = \begin{bmatrix} \boldsymbol{\rho}_1^H \boldsymbol{\rho}_1 & 0 & \cdots & 0 \\ 0 & \boldsymbol{\rho}_2^H \boldsymbol{\rho}_2 & \cdots & 0 \\ \vdots & \vdots & \ddots & \vdots \\ 0 & 0 & \cdots & \boldsymbol{\rho}_M^H \boldsymbol{\rho}_M \end{bmatrix}. \tag{18}$$

When the matched filter is applied to the measurements received, the estimate of the  $i$ th target is

$$\begin{aligned}\hat{\gamma}_i &= (\mathbf{w}_i^{\text{corr}})^H \mathbf{r} \\ &= \gamma_i + \sum_{j, j \neq i} (\mathbf{w}_i^{\text{corr}})^H \boldsymbol{\rho}_j \gamma_j + (\mathbf{w}_i^{\text{corr}})^H \mathbf{n}.\end{aligned}\quad (19)$$

As seen in (19), error in the matched filtering operation comes from two terms. The first error component is represented by the summation term. This is the error due to clutter because of correlation between the desired target and other scatterers. The second error component is shown in the last term of (19) as the error component due to noise. The matched-filter vector, however, has the smallest magnitude of any filter vector that gives  $\gamma_i$  as its expected result. Therefore, the matched filter has the least noise power at its output of any linear filter. While the matched filter maximizes output SNR, it does not account for clutter in any manner. In cases that are clutter limited rather than noise limited, the matched filter does not provide optimal estimates. However, it is this lack of dependence on clutter that also makes the matched-filter vectors the least computationally expensive to generate.

An important interpretation of the matched filter applied to angle information is that the matched filter is equivalent to beamforming. The matched filter maximizes SNR by focusing, or steering, the array pattern directly toward each target it is estimating. Range-Doppler processing reduces all but the target and its range-Doppler ambiguities. The spatial matched filter then forms a beam that maximizes array gain in the direction of the desired target and simultaneously attenuates range-Doppler sidelobes and ambiguities that fall outside the array's mainlobe.

### B. Sparse Arrays

The microsat concept calls for placing each receive aperture on its own, smaller satellite. Furthermore, the orbital dynamics of formation flying require the satellites to have significant, random spacing between them. Therefore, the microsat array is sparsely populated, and different spatial processing must be applied. Fig. 4(a) shows a sparse array configuration. It is seen in Fig. 4(a) that the spacing between apertures is not regular or periodic; the apertures are randomly placed in three dimensions. This represents control of the array structure by orbital dynamics rather than antenna array design and does not assume that those orbital dynamics produce a formation that is either linear or planar. It is assumed that the apertures have the same azimuth and elevation angles at boresight; therefore, the satellites' illumination patterns on the ground are assumed to be identical.

The sparse, randomly sampled array has significant consequences on the algorithms applied to the spatial data. As seen in Fig. 4(b), matched filtering has become less effective because the array pattern has sidelobes that fall on range-Doppler ambiguities. This is easily understood by viewing the ambiguity functions in Fig. 5(a)–(c). In Fig. 5(a), the range-Doppler ambiguity function is again shown. Instead of the well-defined mainlobe, nulls, and sidelobes seen in Fig. 2(b), the array pattern in Fig. 5(b) has a smaller mainlobe due to the increased array spatial extent and a random pattern of sidelobes and grating

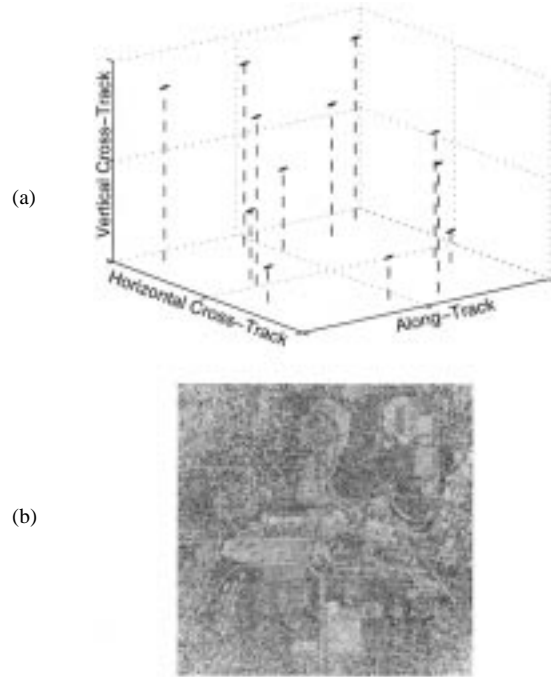


Fig. 4. Results from a sparse array configuration. (a) The sparse, randomly located receiver array used with matched-filter processing to generate the SAR image in (b).

lobes. Because the array pattern behaves in this way, in general the nulls of the spatial pattern will not lie on ambiguities in range-Doppler. Unambiguous targets in range-Doppler are still unambiguous overall, but ambiguities in range-Doppler have varying degrees of correlation depending on where they fall in the spatial pattern. The result is the total ambiguity function shown in Fig. 5(c). The correlation matrix for the sparse, multiple-aperture case was also calculated and is shown in Fig. 5(d). The perfect matrix occurs when all targets are completely uncorrelated. In this ideal case, the measurement vectors are orthogonal to each other, and the correlation matrix is in the form of an identity matrix. All dark off-diagonal elements represent deviation from the ideal case; therefore, it is seen by comparing Figs. 2(d) and 5(d) that, as expected, the situation has degraded in the sparse case.

### C. Maximum-Likelihood Filter

If the vector of measurements,  $\mathbf{r}$ , is defined as before, and the vector of noise values,  $\mathbf{n}$ , is jointly Gaussian, complex noise with zero mean and a covariance matrix given by  $\mathbf{K}_n$ , then the conditional density of the observation and RCS vectors becomes

$$p(\mathbf{r}/\boldsymbol{\gamma}) = \frac{1}{\sqrt{|2\pi\mathbf{K}_n|}} \exp \left[ -\frac{1}{2}(\mathbf{r} - \mathbf{P}\boldsymbol{\gamma})^H \mathbf{K}_n^{-1} (\mathbf{r} - \mathbf{P}\boldsymbol{\gamma}) \right]. \quad (20)$$

Using (20), the maximum-likelihood (ML) estimator is obtained by maximizing the argument of the exponential function

$$\max_{\boldsymbol{\gamma}} -\frac{1}{2}(\mathbf{r} - \mathbf{P}\boldsymbol{\gamma})^H \mathbf{K}_n^{-1} (\mathbf{r} - \mathbf{P}\boldsymbol{\gamma}). \quad (21)$$

The ML estimator then becomes

$$\mathbf{W}_{\text{ml}} = (\mathbf{P}^H \mathbf{K}_n^{-1} \mathbf{P})^{-1} \mathbf{P}^H \mathbf{K}_n^{-1}. \quad (22)$$

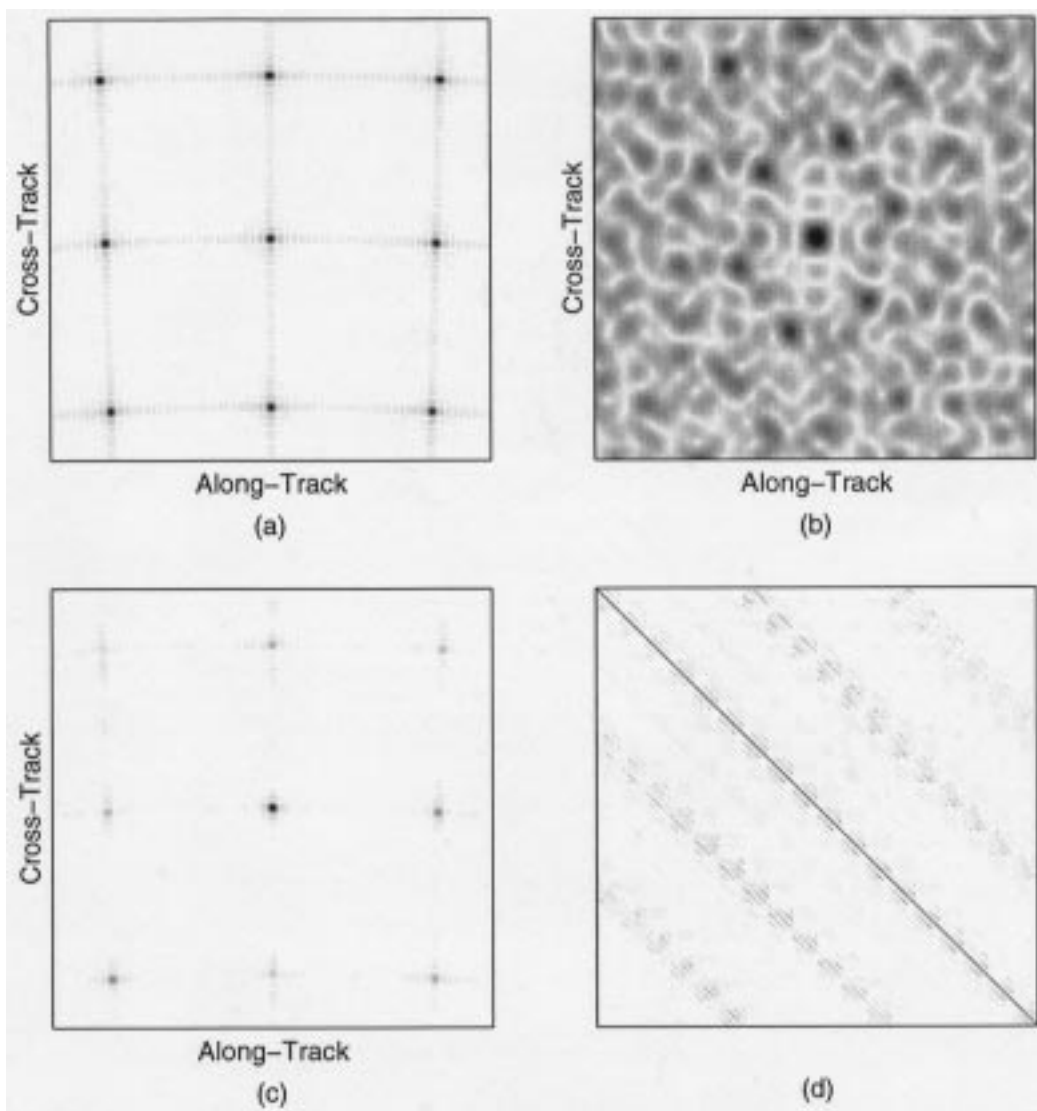


Fig. 5. (a) The range-Doppler ambiguity function and (b) receive array pattern for the sparse array combine to give the (c) total ambiguity function. Ambiguities seen in (c) also appear as off-diagonal components in (d).

Next, if it is assumed that the noise samples are independent, then the noise covariance matrix is diagonal

$$\mathbf{K}_n = \sigma_n^2 \mathbf{I} \quad (23)$$

where  $\mathbf{I}$  is the identity matrix. The ML estimator then reduces to

$$\mathbf{W}_{ml} = \mathbf{P}^{\sim 1} \quad (24)$$

where  $(\cdot)^{\sim 1}$  denotes the pseudoinverse operation. In order to obtain good results when the spatial array is sparsely sampled, it is clear that ambiguities in range-Doppler must fall on nulls in the spatial pattern. The ML estimator forces this condition on the array pattern.

The estimate of the  $i$ th pixel's RCS due to the ML filter is then

$$\hat{\gamma}_i = (\mathbf{w}_i^{ml})^H \mathbf{r} = \gamma_i + (\mathbf{w}_i^{ml})^H \mathbf{n}. \quad (25)$$

Comparing the forms of (25) and (19), it is seen that the clutter term is absent in (25). The last term in (25), however, becomes

important. If  $\mathbf{P}$  is ill conditioned, then the magnitude of the weight vectors that make up  $\mathbf{W}_{ml}$  can be very large and any noise present in the measurements will be significantly amplified. Thus, SNR and the condition of  $\mathbf{P}$  become crucial factors in determining the quality of the SAR image obtained through the ML filter.

The condition of  $\mathbf{P}$  can be improved by adding more apertures because the spatial degrees of freedom will increasingly exceed the number of range-Doppler ambiguities. The effect is the same as what is seen in array pattern synthesis where the degrees of freedom largely determine how much the mainlobe distorts when nulls are enforced. More apertures correspond to more degrees of freedom, and more degrees of freedom correspond to maintaining gain on the target without sacrificing the number and depth of array pattern nulls.

Results for the ML filter are shown in Fig. 6. Fig. 6(a) shows the output of the ML filter when the SNR of the measurements is high. In this case, range-Doppler ambiguities are nulled by the ML weight vector with excellent results. In Fig. 6(b), however, the SNR is low. Since the pseudoinverse operation calculates

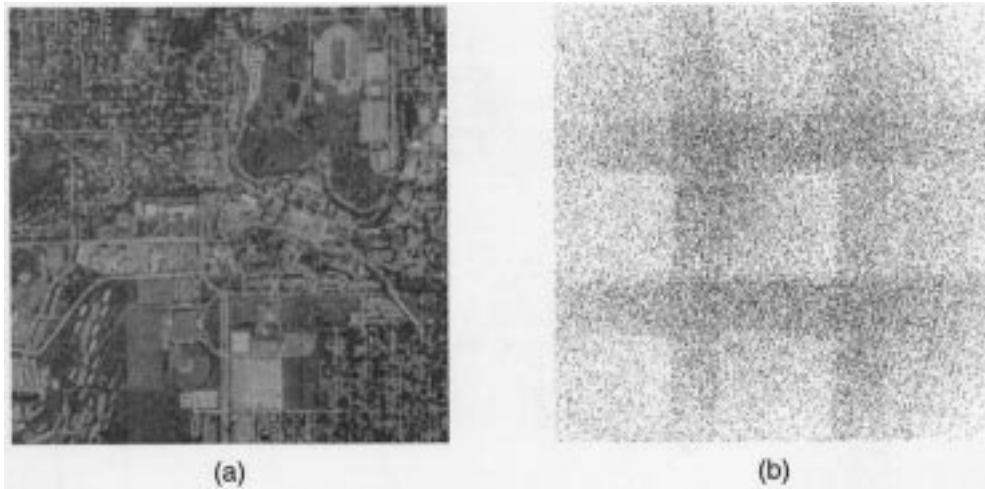


Fig. 6. ML processing of a sparse, random array for (a) high SNR and (b) low SNR.

weight vectors that are large in magnitude, the high noise power is amplified and overwhelms the output.

The ML filter maximizes the signal-to-clutter ratio (SCR). In cases where the number of receivers is significantly larger than the number of range-Doppler ambiguities, the ML filter produces an excellent result. Disadvantages of the filter include poor results when the SNR is low and increased computation required to calculate  $\mathbf{W}$  due to the pseudoinverse operation.

#### D. MMSE Filter

The minimum mean-squared error (MMSE) method uses statistical properties of the targets and noise to calculate the filter that achieves the best compromise between output SCR and SNR. The MMSE filter maximizes the signal-to-interference ratio (SIR) where interference is the sum of noise and clutter. The MMSE filter, therefore, is the mathematically optimum compromise between the correlation and ML filters.

The derivation of the linear MMSE filter begins with the orthogonality principle, which can be expressed as [25]

$$\mathbf{E}[(\hat{\boldsymbol{\gamma}} - \boldsymbol{\gamma})^H \mathbf{M} \mathbf{r}] = 0 \quad (26)$$

where  $\mathbf{M}$  is used to represent all linear combinations of the data,  $\mathbf{r}$ . Beginning with (26) and following through gives the MMSE operator

$$\mathbf{W}_{\text{mmse}} = \mathbf{E}[\boldsymbol{\gamma} \boldsymbol{\gamma}^H] \mathbf{P}^H (\mathbf{P} \mathbf{E}[\boldsymbol{\gamma} \boldsymbol{\gamma}^H] \mathbf{P}^H + \mathbf{E}[\mathbf{nn}^H])^{-1}. \quad (27)$$

If the elements of the RCS vector,  $\boldsymbol{\gamma}$ , are assumed to be independent with identical statistics, and  $\mathbf{E}[\mathbf{nn}^H]$  is recognized as the noise covariance matrix,  $\mathbf{K}_n$ , then (27) reduces to

$$\mathbf{W}_{\text{mmse}} = \gamma_t^2 \mathbf{P}^H (\gamma_t^2 \mathbf{P} \mathbf{P}^H + \mathbf{K}_n)^{-1} \quad (28)$$

where the expected value of the squared RCS magnitude for each target is  $\gamma_t^2 = \mathbf{E}[\gamma_i^H \gamma_i]$ .

Looking at (28) gives some important insight into the behavior of the MMSE filter. First, in a low-noise or zero-noise case,  $\mathbf{K}_n$  will be negligible and  $\mathbf{W}_{\text{mmse}}$  becomes

$$\mathbf{W}_{\text{mmse}} \approx \gamma_t^2 \mathbf{P}^H \frac{1}{\gamma_t^2} (\mathbf{P}^H)^{-1} \mathbf{P}^{-1} = \mathbf{P}^{-1} \quad (29)$$

which is the same as the ML filter. In the low-noise case, therefore, the MMSE filter maximizes SCR. In the high-noise case,  $\mathbf{K}_n$  dominates and  $\mathbf{W}_{\text{mmse}}$  becomes

$$\mathbf{W}_{\text{mmse}} \approx \gamma_t^2 \mathbf{P}^H \mathbf{K}_n^{-1} = \frac{\gamma_t^2}{\sigma_n^2} \mathbf{P}^H. \quad (30)$$

The filter representation in (30) is a vector in the same direction as the matched filter. An importance difference, however, is that the MMSE filter becomes inversely proportional to the noise variance. Hence, as the noise variance approaches infinity, the magnitude of the MMSE filter approaches zero. Therefore, inherent in the equation for the MMSE filter is the concession that, in the presence of overwhelming noise, it is best to estimate the RCS values not by the measurements, but by the statistical properties of the targets.

Fig. 7 shows the results for the three filters when applied to three different SNR cases: low SNR, moderate SNR, and infinite SNR. The apertures for Fig. 7 are in a sparse, randomly located, 12-element array. It is seen that in the infinite-SNR case, the ML and MMSE filters produce the same results. The matched filter, however, produces results that are much worse because it remains clutter limited. In the low-SNR case, the matched and MMSE filters produce similar results, but the matched result is brighter. This is because the matched filter does not reduce its magnitude as noise is increased, and the brightness increases with increased noise power. The ML filter becomes unstable in the low-SNR case. Its magnitude for some targets is very large because it must compensate for loss of gain due to strict enforcement of the null constraints. In the moderate-SNR case, the MMSE filter again produces better results than either the ML or matched filter.

The primary advantage of the MMSE filter is that it, by definition, provides the minimum mean-squared error in all noise

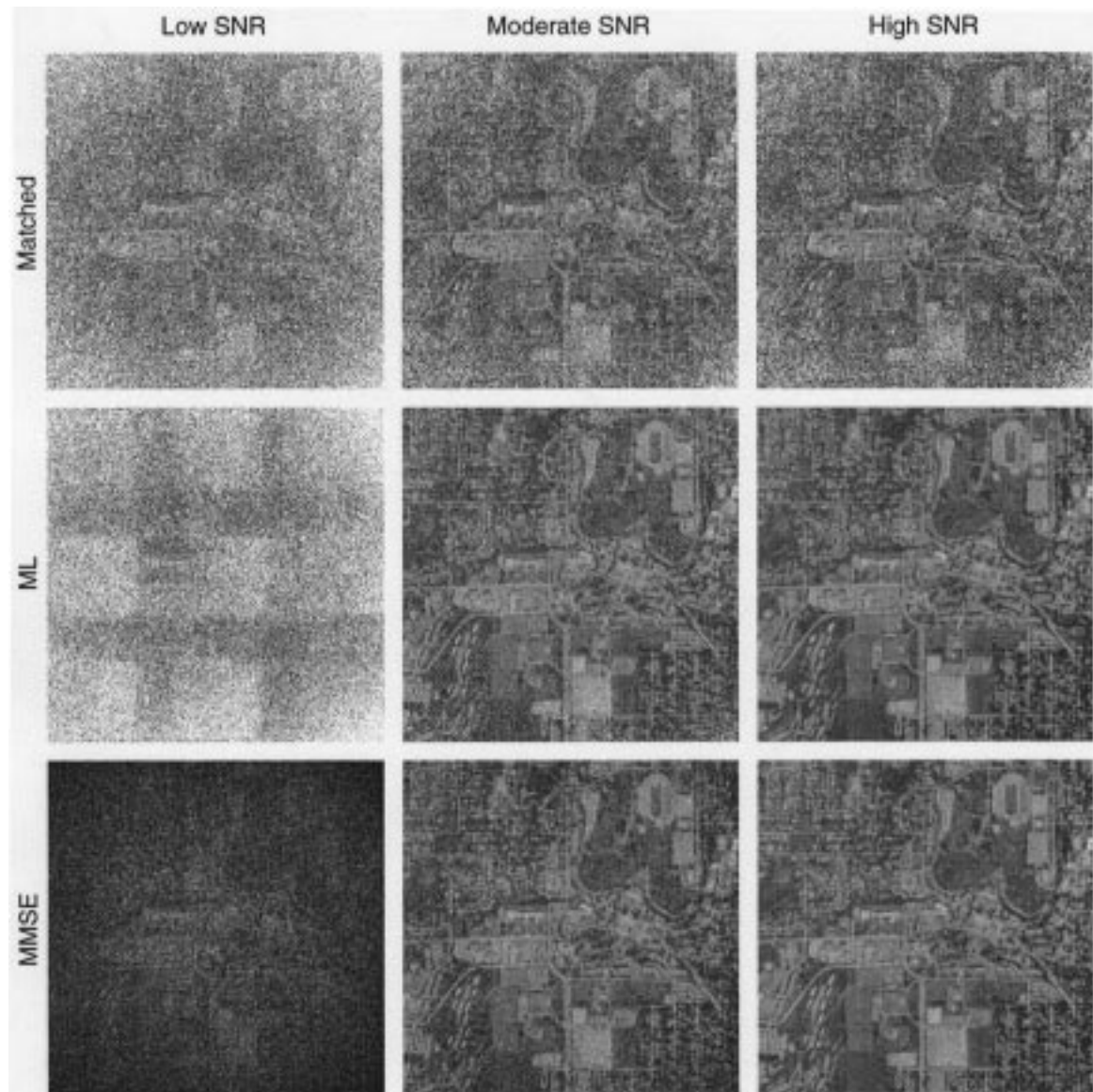


Fig. 7. SAR images from a sparse, random array with 12 receive apertures. Comparison of the correlation, ML, and MMSE filters for low, moderate, and infinite SNR.

and clutter scenarios. The filter accounts for the statistical properties of the targets and noise in order to maximize SIR. The cost of implementing the MMSE filter is increased computation for calculating  $\mathbf{W}$  compared to the matched filter.

## V. NUMERICAL RESULTS

The images presented thus far pictorially demonstrate the advantages of multiple receive apertures and ML or MMSE spatial processing, but it is also informative to assess performance of the different algorithms numerically. Several error curves are presented that demonstrate the performance of the three algorithms versus different variables. The error criterion is the mean-squared error (MSE) of the pixel magnitudes normalized by the image's mean-squared pixel magnitude

$$\text{MSE} = \frac{(\hat{\gamma} - \gamma)^H (\hat{\gamma} - \gamma)}{\gamma^H \gamma}. \quad (31)$$

It is mentioned here that the ML and MMSE filters could be calculated using the entire measurement vectors of all targets, including time, frequency, and spatial measurements. However, this would require inversion of an extremely large matrix. Since this is unrealistic, it has been tacitly assumed throughout this paper that matched filtering is applied in the time and frequency domains, and the more complex filters are reserved for spatial processing. Once the time–frequency matched filter is applied, it is only necessary to force the spatial weight vector to null range-Doppler ambiguities because these are the targets that cause significant problems when they come through sidelobes of the spatial pattern. In this implementation, spatial processing is a second layer that nulls out those clutter targets that were not already filtered by the range-Doppler processing. Some effects of processing the data in this way can be seen in the numerical results of this section and will be pointed out as necessary.

First, the effect of SNR on performance is investigated. Fig. 8 shows the mean-squared error as a function of input SNR and

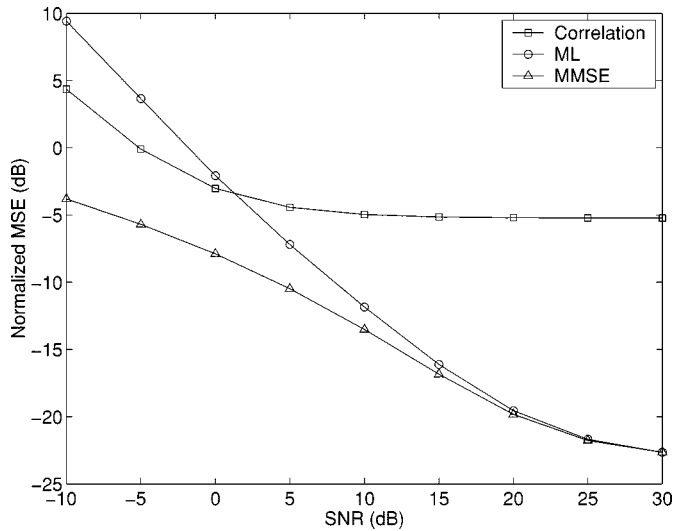


Fig. 8. Correlation, ML, and MMSE filter performance versus SNR for a 12-receiver, sparse, random array.

clearly validates the conclusions that have been stated about the performance of the three filters. Most important, the MMSE filter has the lowest error at every SNR. Also of importance is the rapid increase in error as SNR decreases for the ML filter and the flattening of the matched filter curve for high SNR. The flat curve for the matched filter as SNR increases shows that the matched filter is clutter limited; therefore, improving SNR does not improve the results. The ML and MMSE curves begin to flatten at lower error and higher SNR than the matched filter. The error floor is due to range-Doppler matched filtering. The level of range-Doppler sidelobes due to matched filtering in time and frequency determines the best achievable performance when the SNR is high. If the ML and MMSE filters were applied to the entire data set in time, frequency, and space, the error would continue to decrease for increasing SNR. Application of the ML and MMSE filters in the spatial domain only, however, does yield significant improvement over the matched filter as shown by the right side of Fig. 8.

Another important factor that has not yet been mentioned is the accuracy of information about the physical scenario. Since the physics must be known in order to calculate the measurement vectors, any deviation from the expected scenario will introduce error in the results. Fig. 9 shows the behavior of the estimation error versus one particular deviation: receiver positioning error. In this simulation, the filters were calculated using assumed receiver positions. When the radar measurements were simulated, however, the receiver locations were randomly deviated from the assumed locations according to a Gaussian distribution of standard deviation,  $\sigma_p$ , in each dimension. The standard deviation of the total positioning error for each receiver was then

$$\sigma_e = \sqrt{3}\sigma_p. \quad (32)$$

Fig. 9 shows estimation error versus  $\sigma_e$  for simulations performed at infinite SNR. The matched filter results vary little versus amount of positioning error. However, since placing nulls requires accurate phase information, the ML and MMSE results are very sensitive to positioning error.

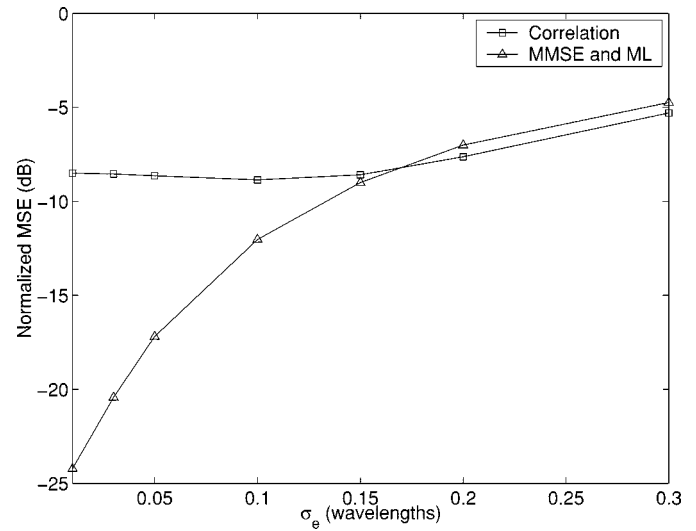


Fig. 9. Correlation, ML, and MMSE filter performance versus antenna positioning error for a 12-receiver, sparse, random array and infinite SNR.

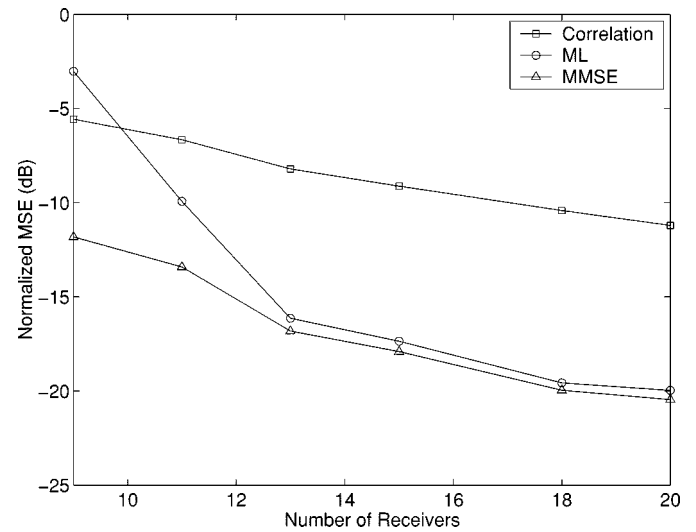


Fig. 10. Correlation, ML, and MMSE filter performance versus number of receive apertures for a sparse, random array and moderate SNR.

It was mentioned earlier that forming nulls in the spatial pattern requires enough degrees of freedom. More degrees of freedom allows forming the required nulls without sacrificing gain on the target. Hence, it is expected that estimation error will decrease as the number of apertures increases. Fig. 10 demonstrates this result. The estimation error versus number of receivers in Fig. 10 is relatively flat for the matched filter because it only has one constraint: that the gain on the target be maximized. The entire range from nine to 20 receivers provides enough degrees of freedom to satisfy this one constraint. The ML and MMSE filters, however, have nine constraints (the target and eight ambiguities). Therefore, as the number of receive apertures is increased from nine to 20, the degrees of freedom increase significantly. The slight improvement seen for each of the filters as the number of receive apertures is increased from 13 to 20 is due to improving SNR. This SNR improvement occurs because each additional aperture increases the amount of signal energy collected.

## VI. CONCLUSION

We demonstrated the utility of multiple receive apertures. The spotlight area, or swathwidth, of a SAR system is fundamentally limited by the amount of information that can be collected at a given resolution, and multiple receive apertures mitigate this situation by adding independent angle-of-arrival information. We presented a sparsely populated array with randomly placed elements and discussed the motivation for such an array in space. We also presented additional algorithms for processing the angle-of-arrival information and applied them to multiple receive aperture simulations. We showed results produced by the three different algorithms for varying SNRs and investigated performance versus the factors of SNR, receive-aperture positioning accuracy, and number of receive elements.

The results presented in this paper demonstrate both the needs for and methods of applying multiple receive apertures to obtain wide-area SAR images. Future spaceborne systems of the microsat concept are being studied, and this paper demonstrates how the measurements from such systems can be processed effectively. Several factors will affect this processing. One of the most important factors is the number of receivers. In order for a system such as the one proposed to work, there must be enough receive apertures to null all range-Doppler ambiguities as well as keep the mainlobe on the target. A sufficient number of receivers ensures that the ML and MMSE algorithms will not produce unstable results in the presence of noise; therefore, any operational system based on the constellation concept should have enough receivers that some gain can be maintained while still enforcing nulls in the array pattern. The SNR received by a sparsely populated, spaceborne array affects the processing that should be used. In situations where the received SNR is high enough, the improved performance of the ML and MMSE filters justify their added computational expense.

Another important factor is the ability to position the receive apertures accurately. As with any pattern synthesis problem where nulls are desired, the relative phase shifts between elements are the dominant components in the algorithm. Ability to estimate these phase shifts accurately is crucial. Although the results presented in Fig. 9 are for only one particular microsat constellation, the improvement shown by the ML and MMSE solutions for absolute positioning errors of one-tenth of a wavelength or less is probably a good rule of thumb. Again, a benefit of having extra receive apertures becomes apparent, as increasing the number of apertures will ease positioning accuracy requirements for a given error level. However, the ability to obtain accurate knowledge of the receiver positions is an essential technological requirement for any operational implementation of the constellation concept.

The MMSE solution is the most robust solution. It maximizes SCR in clutter-limited cases and SNR in noise-limited cases. Its computational expense is significantly more than for the matched filter, but only slightly more than for the ML filter. Furthermore, the added computation is not data dependent, and the MMSE filter can be calculated before data is collected. In moderate-to-high-SNR cases with low positioning error, the results produced by the MMSE filter certainly justify its added computational burden.

## REFERENCES

- [1] C. Elachi, *Spaceborne Radar Remote Sensing: Applications and Techniques*. New York: IEEE Press, 1988.
- [2] F. K. Li and W. T. K. Johnson, "Ambiguities in spaceborne synthetic aperture radar systems," *IEEE Trans. Aerosp. Electron. Syst.*, vol. AES-19, pp. 389–396, May 1983.
- [3] S. W. McCandless, "SAR in space—The theory, design, engineering and application of a space-based SAR system," in *Space-Based Radar Handbook*, L. J. Cantafio, Ed. Norwood, MA: Artech House, 1989, ch. 4.
- [4] K. Tomiyasu, "Image processing of synthetic aperture radar range ambiguous signals," *IEEE Trans. Geosci. Remote Sensing*, vol. 32, pp. 1114–1117, Sept. 1994.
- [5] —, "Performance of a proposed spaceborne synthetic aperture radar with variable antenna height," *IEEE Trans. Geosci. Remote Sensing*, vol. 28, pp. 609–613, July 1990.
- [6] —, "Conceptual performance of a satellite borne, wide swath synthetic aperture radar," *IEEE Trans. Geosci. Remote Sensing*, vol. GE-19, pp. 108–116, Apr. 1981.
- [7] F. T. Ulaby, R. K. Moore, and A. K. Fung, *Microwave Remote Sensing: Active and Passive*. Norwood, MA: Artech House, 1982, vol. 2, ch. 9.
- [8] R. K. Moore, "Scanning spaceborne synthetic aperture radar with integrated radiometer," *IEEE Trans. Aerosp. Electron. Syst.*, vol. AES-17, pp. 410–421, May 1981.
- [9] D. L. Evans, Ed., *Spaceborne Synthetic Aperture Radar: Current Status and Future Directions*. Washington, DC: NASA, 1995.
- [10] A. Moreira, J. Mittermayer, and R. Scheiber, "Extended chirp scaling algorithm for air- and spaceborne SAR data processing in stripmap and ScanSAR imaging modes," *IEEE Trans. Geosci. Remote Sensing*, vol. 34, pp. 1123–1136, Sept. 1996.
- [11] A. Currie and M. A. Brown, "Wide-swath SAR," *Proc. Inst. Elect. Eng. F*, vol. 139, no. 2, pp. 122–135, Apr. 1992.
- [12] V. Mrstik, "Agile-beam synthetic aperture radar opportunities," *IEEE Trans. Aerosp. Electron. Syst.*, vol. 34, pp. 500–507, Apr. 1998.
- [13] R. K. Moore, "Trade-off between picture element dimensions and non-coherent averaging in side-looking airborne radar," *IEEE Trans. Aerosp. Electron. Syst.*, vol. AES-15, pp. 697–708, Sept. 1979.
- [14] R. L. Fante, "Adaptive nulling of SAR sidelobe discretions," *IEEE Trans. Aerosp. Electron. Syst.*, vol. 35, pp. 1212–1218, Oct. 1999.
- [15] A. Moreira, "Real-time synthetic aperture radar (SAR) processing with a new subaperture approach," *IEEE Trans. Geosci. Remote Sensing*, vol. 30, pp. 714–722, July 1992.
- [16] J. Mittermayer, A. Moreira, and O. Loffeld, "Spotlight SAR data processing using the frequency scaling algorithm," *IEEE Trans. Geosci. Remote Sensing*, vol. 37, pp. 2198–2214, Sept. 1999.
- [17] M. A. Richards, "Synthetic aperture processing," in *Airborne Pulsed Doppler Radar*, G. Morris and L. Harkness, Eds. Boston, MA: Artech House, 1996, ch. 10.
- [18] C. Prati and F. Rocca, "Improving slant-range resolution with multiple SAR surveys," *IEEE Trans. Aerosp. Electron. Syst.*, vol. 29, pp. 135–143, Jan. 1993.
- [19] A. Herique, L. Phalippou, S. Ramongassie, and C. C. Lin, "High resolution SAR constellation for risk management," in *CEOS SAR Workshop Proc.*, Toulouse, France, Oct. 1999.
- [20] M. Younis and W. Wiesbeck, "SAR with digital beamforming on receive only," in *1999 IEEE Geoscience and Remote Sensing Symp. Proc.*, vol. 3, Hamburg, pp. 1773–1775.
- [21] J. M. Stiles and N. Goodman, "Processing of multi-aperture SAR to produce fine-resolution images of arbitrarily large extent," in *Proc. 2001 IEEE Radar Conf.*, Atlanta, GA, May 2001, pp. 451–456.
- [22] M. Martin and M. Stallard, "Distributed satellite missions and technologies—the TechSat 21 program," in *Proc. AIAA Space Technology Conf. Exposition*, Albuquerque, NM, Sept. 1999, AIAA 99-4479.
- [23] A. Das, R. Cobb, and M. Stallard, "TechSat 21: A revolutionary concept in distributed space based sensing," in *Proc. AIAA Defense and Civil Space Programs Conf. Exhibit*, Huntsville, AL, Oct. 1998, AIAA 98-5255.
- [24] N. Levanon, *Radar Principles*. New York: Wiley, 1988.
- [25] D. H. Johnson and D. E. Dudgeon, *Array Signal Processing: Concepts and Techniques*. Englewood Cliffs, NJ: Prentice-Hall, 1993.



**Nathan A. Goodman** (S'98) received the B.S. and M.S. degrees in electrical engineering from the University of Kansas, Lawrence, in 1995 and 1997, respectively. He is currently pursuing the Ph.D. degree in electrical engineering at the Radar Systems and Remote Sensing Laboratory at the University of Kansas.

In August 1996, he joined Texas Instruments, Dallas, TX, as an RF Systems Engineer. His research interests are in radar systems and signal processing, and his current research is on SAR and

MTI processing of sparse arrays with particular application to a space-based constellation of radar satellites.

Mr. Goodman was awarded the Madison A. and Lila Self Graduate Fellowship upon returning to the University of Kansas in 1998.

**Sih Chung Lin**, photograph and biography not available at the time of publication.

**Devindran Rajakrishna** received the B.S. degree in electrical engineering (Honors) from The University of Iowa, Iowa City, in 1996, and the M.S. degree in electrical engineering from The University of Kansas, Lawrence, in 1998.

He is currently Senior Member of Technical Staff at Tellabs, Inc. Lisle, IL. His current work area is in systems engineering for a digital cross-connect.



**James M. Stiles** (S'91-M'95-SM'97) received the B.S. degree in electrical engineering from The University of Missouri, Columbia, in 1983, the M.S. degree in electrical engineering from Southern Methodist University, Dallas, TX, in 1987, and the Ph.D. degree in electrical engineering from The University of Michigan, Ann Arbor, in 1996.

From 1983 to 1990, he was a Microwave Systems Design Engineer for Texas Instruments, Dallas, TX, and from 1990 to 1996, he was a Graduate Research Assistant in the Radiation Laboratory at the University of Michigan.

Since 1996, he has been an Assistant Professor at the University of Kansas, Lawrence, where he is a member of the Radar Systems and Remote Sensing Laboratory (RSL). His research interests include radar remote sensing of vegetation, propagation and scattering in random media, ground-penetrating radar, and radar signal processing.